



Evolution characteristics of microstructure and properties in AZ31 alloy during high cycle fatigue processes

Jiang-ping YU, Xi-yan ZHANG, Yang SHU, Li TAN, Rui-sen YIN

School of Materials Science and Engineering, Chongqing University, Chongqing 400030, China

Received 21 April 2016; accepted 8 October 2016

Abstract: In order to investigate the microstructure and properties evolution of the AZ31 magnesium alloy in different cycles (including 10^4 (sample 1), 10^6 (sample 2) and none (sample 3, no fatigue tests on the samples)) of high cycle deformation, the scanning electron microscopy (SEM) and electron back-scattered diffraction technique (EBSD) were fully used. It is found that many $\{10\bar{1}2\}$ tension twins (near 21%, volume fraction), a few $\{10\bar{1}1\}$ compression twins and $\{10\bar{1}1\}-\{10\bar{1}2\}$ secondary twins are generated during tension–compression cyclic deformation. The volume fractions of $\{10\bar{1}2\}$ twins in samples 1, 2 and 3 are 8%, 21% and 4%, respectively. By analyzing the fatigue fracture of the samples, larger area of fatigue striations and cleavage fracture in samples are also observed, as well as the shallower dimples. The twin laminae are likely to occur in the crack initiation zone while dimples are in the final fracture region and the dimple size increases with the increase of the cycle number. The dimple diameters of samples 1, 2 and 3 are 14.8, 31.2 and 8.5 μm , respectively. It turns out that both the fatigue strength and elongation of the samples slightly decrease with increasing the cycle number.

Key words: AZ31 alloy; fatigue deformation; microstructural evolution; fracture morphology

1 Introduction

In the 21st century, the promising materials are thought to be high efficiency, energy saving, and have the minimality to the mass of structural elements and the reduction of the environmental loads to the globe [1,2]. Luckily, magnesium alloys, owing to some preeminent properties such as low density, high specific strength and stiffness, high damping capacity, and good recyclability, have been attracting more and more attention and research as one of the most promising materials regarded as “green” for structural materials used in automotive and aerospace industries, and other industrial sectors [3,4]. In the wake of developments in extruding and rolling technology nowadays, wrought magnesium alloys are likely to make full use of mechanical capacities under high cyclic loading in all various kinds of working environment, thus resulting in fatigue failure inevitably. Many researchers studied the mechanism of fatigue deformation. MORITA et al [5] found that crack initiated on the specimen surface regardless of specimen direction. CHAMOUS and PANTELAKIS [6] found a

smooth transition in $S-N$ curves of hot-rolled Mg alloys AZ31 and AZ61. FONTE and FREITAS [7] found the intersection of steady torsion on fatigue crack growth of semi-elliptical cracks in shafts under rotation bending and steady torsion. HOSSEINI and LIMOOEI [8] indicated that the notched material presented a different sensitivity when the specimens were subjected to high and low cycle fatigue tests. However, YANG et al [9] ascribed the cycle fatigue in AZ31 Magnesium alloy to deformation twins. There is no consistence on the effect of loading cycle number on the deformation mechanism.

Wrought magnesium alloys are truly free of casting defects such as casting porosity and microscopic shrink hole in comparison with casting alloys [1]. More importantly, wrought magnesium alloys possess good fatigue properties and are proper for the study of fatigue mechanism of magnesium alloys [10,11]. For the application of the wrought alloys, it is urgent to evaluate fatigue mechanisms of magnesium alloys. On one hand, due to the hexagonal close-packed structure and limited number of slip systems, the dominant deformation mechanisms for most magnesium alloys in ambient air are dislocation slip and deformation twinning [12],

including two primary types of $\{10\bar{1}2\}\langle 10\bar{1}1\rangle$ extension and $\{10\bar{1}1\}\langle 10\bar{1}2\rangle$ contraction at room temperature [13], resulting in poor formation. On the other hand, the study on the fatigue deformation of magnesium alloys nowadays is just the behavior of macroscopic cyclic deformation and fatigue fracture [14], ignoring that the induced fatigue deformation in essence is microstructure evolution. It is widely believed that the fatigue properties of AZ31 magnesium alloy during the fatigue test were related to the number of high cycles. Therefore, in this study, different loading cycles during the fatigue test were utilized, aiming at finding the laws on fatigue between loading cycles and microstructure of the magnesium alloy. Some experimental studies revealed the rules about high cycle fatigue and fatigue crack propagation behavior. The relationship between the microstructure and different loading cycle processes was discussed as well.

2 Experimental

In order to characterize the relationship between the evolution of microstructure and the variation of mechanical properties of AZ31 magnesium alloy during high cycle fatigue tests, experimental procedures were designed as follows.

1) Through a sinusoidal waveform stress-control mode with a frequency close to 97.4 Hz, the fatigue tests were carried out at room temperature by PLG-100 high-frequency electromagnetic resonance fatigue test system with a capacity of 100 kN. Using specific high cycles (i.e., 10^4 and 10^6 , none and named samples 1, 2 and 3, respectively), the original stress levels were 70 MPa by means of cycle-symmetric ($R=-1$) loads. Tests were stopped when the specimens were fractured or exceeded specified cycles without evident damage. Samples with different loading numbers were cut from the as-rolled AZ31 sheet along the rolling direction (RD) at room temperature. The dimensions of the specimens for the fatigue tests are shown in Fig. 1. In order to delay the crack initiation, the specimens were polished with metallography sand paper (800, 1000, 1200 grit).

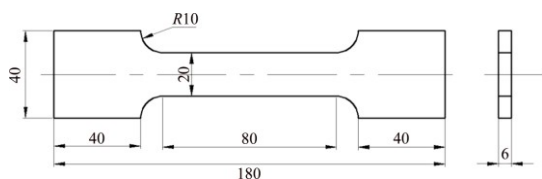


Fig. 1 Geometry of fatigue specimen (unit: mm)

2) The quasi-static tensile tests were performed on AZ31 samples after fatigue tests up to failure with the help of SHIMADZU AG-X10KN machine at an initial strain rate of 0.01 s^{-1} and room temperature. Specimens

were cut from the fatigue specimens under specific cycles and the original one. The sampling method of tensile samples is shown in Fig. 2.

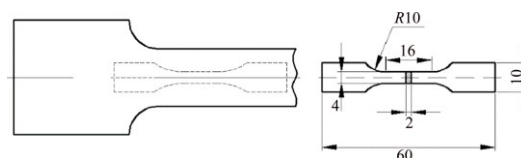


Fig. 2 Tension specimen cut from fatigue specimen after specific cycles (unit: mm)

After tensile test, the TESCAN VEGA 3 was applied to investigating the fracture morphology of the samples. Scanning electron microscopy–electron back-scattered diffraction (SEM–EBSD) was utilized to analyze the microstructure and texture of samples. The deformation within the samples under uniaxial tension was of inhomogeneity, so EBSD data were acquired from the center of the fracture cross section of the sample. EBSD scans were performed by FEI Nova 400 FEG–SEM and EBSD information was acquired with Channel 5 software. The specimens for EBSD were prepared by standard metallographic polishing, then electro-polished by using the commercial AC 2 electrolyte for 60 s at 20 V and 20 °C.

3 Results and discussion

3.1 Tensile mechanical properties of different numbers of cycles

The engineering stress–strain curves of samples tested at a strain of 0.01 s^{-1} are shown in Fig. 3. The deformation of the AZ31 magnesium alloy is quite different with the increase of the cycles. Obvious differences in the tensile and yield strengths between samples 1 and 2 may be caused by the formation of the strong base texture, which are not in accordance with those of sample 1. It can also be seen that the strength and plasticity of sample 2 after fatigue deformation are strongly higher than those of sample 1, but lower than those of sample 3 (the original one). However, after the cycles to some extent, the stress slope comes into relative gentleness, which means cycle softening. At the same time, the ultimate compressive stress of sample 2 is also higher than that of sample 1. It is well received that the fatigue property of the material is closely related to the static mechanical properties, that is to say, high cycle performance fatigue depends on the strength, while low cycle fatigue performance depends on the plastic of materials. In view of this consideration, the high cycle fatigue properties of sample 2 are slightly higher than those of sample 1. It is known that the microstructure evolution of specimens under cyclic loading is closely

related to the loading cycles, in another way, different cycle numbers cause different levels of work hardening, thus making the diverse characters of samples. In this study, owing to different cycles, the great differences between samples 1 and 2 may account for this phenomenon.

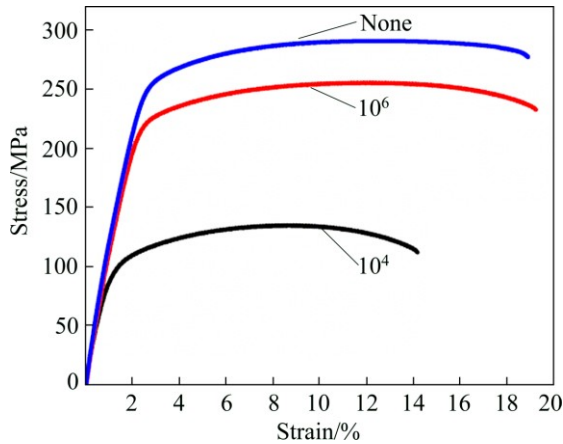


Fig. 3 Tensile flow curves of different samples of different cycling numbers after specific cycles

3.2 Differences of texture at different numbers of cycles

The pole figures of AZ31 magnesium alloy are shown in Fig. 4. The vertical direction is extrusion direction, while the horizontal direction is transverse direction. There is an ellipse-shaped contour of basal plane orientation distribution, indicating that the basal $\langle a \rangle$ slip is easier to occur, which is similar to the results in Refs. [15–18]. There is a strong (0001) texture in the plane after the extrusion with a maximum intensity of 12.6, as shown in Fig. 4, while the $\{11\bar{2}0\}$ tensile twinning texture is rather weak. The concentration of flow strain in shear bands can account for the fact that the texture changes greatly with the increasing cycles of loading. For this reason, the texture of sample 2, which is weaker than that of sample 3, remains quite weak despite the high cycles achieved. The relative weakness of the texture in sample 2 also means that this alloy contains a

higher volume fraction of material in which basal slip may occur.

As is known that two deformation mechanisms like twinning and slip (including basal, prismatic and pyramidal slip) can accommodate more plastic strain. The basal $\langle a \rangle$ dislocations and the pyramidal $\langle c+a \rangle$ dislocations are believed to be the easiest to form [19], while the $\langle c \rangle$ type dislocations in prismatic planes are difficult to activate in magnesium alloy [20]. Due to its low Schmid factor, basal slip is not favored in the textures in the AZ31 alloys. While for RD sample, only basal slip is easily activated [15]. One of the reasons could be ascribed to the effect of grain size, because BETTLES and GIBSON [21] reported that the wrought magnesium alloy with a grain size of 2 μm can obtain symmetric tensile and compressive yield strengths. As the cycles are accumulated, the density of $\langle c+a \rangle$ dislocations increases gradually with increasing the cycle number, and more $\langle c+a \rangle$ dislocations dissociate into $\langle a \rangle$ and $\langle c \rangle$ [22], so pure $\langle c \rangle$ dislocations were generated during these processes. The sessile $\langle c \rangle$ type dislocations are unlikely to produce slip in the $\{11\bar{2}2\}$ planes with increasing the cycle number. These dislocations tangled with each other, contributing to high flow stress and work hardening, and it could also form point defects in the dislocation junctions.

In the high cyclic loading process, the micro-deformation was dominated by the slip system first. After yielding, other slip systems like prismatic $\langle a \rangle$ slip or pyramidal $\langle a \rangle$ slip may be easily activated in samples [18]. In another way, with the increasing cycles, the twinning is likely to occur due to the consolidation of stress of which the slip cannot accommodate the c -axis deformation. As twinning can change the hard orientations to soft ones, this may be one of the reasons why the elongation of sample 2 is higher than that of sample 3, resulting in the easier plastic deformation. Since there are great differences in strengths and elongations of the three samples under tensile loadings, it can be foreseen that the HCP properties of the AZ31 sheet should also display anisotropic features after

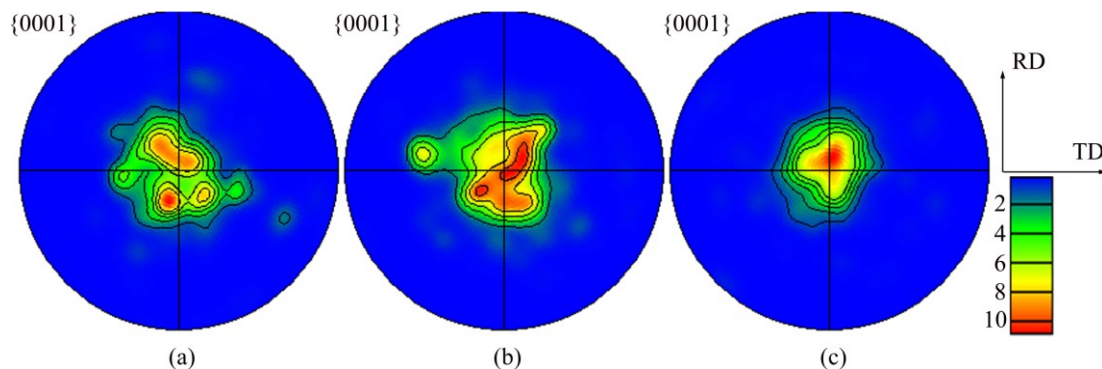


Fig. 4 Pole figures of AZ31 sheet acquired by EBSD at different cycles: (a) 10^4 ; (b) 10^6 ; (c) None

specific tests as discussed in the following parts.

3.3 Microstructure and fracture morphology at different numbers of cycles

The microstructures of the AZ31 magnesium alloys under high cyclic loading were characterized by EBSD and the boundaries of all the deformation twinning modes are identified by color lines seen in Fig. 5 and Table 1. It is interesting that a few of $\{10\bar{1}2\}$ twins exist, in which $\{10\bar{1}2\}$ boundaries have been plotted with red lines, whereas the other types of twin boundaries have been plotted in Fig. 5 with other color lines. The volume fractions of $\{10\bar{1}2\}$ twins in samples 1, 2 and 3 are 8%, 21% and 4% (counted by Channel 5, respectively). The twins in sample 3 may be caused by the sampling preparation.

It is well received that twins disappear or become narrower under reverse loading or reloading because of the polarity characteristic, namely untwinning or detwinning [23]. As a reverse process of twinning, detwinning is different from twinning, one of the great differences is that the activated stress required for untwinning is less than that for twinning nucleation but greater than that of twinning growth [23]. It is the interrelationship between twinning and detwinning that $\{10\bar{1}2\}$ twins in fatigue samples do not increase notably (Fig. 5(c)). When the compression direction is nearly perpendicular to the c -axis, few $\{10\bar{1}1\}$ twin and $\{10\bar{1}1\}$ – $\{10\bar{1}2\}$ secondary twin occur, which can be seen in green lines and blue lines in Figs. 5(a) and (b). The misorientation analysis of twin modes shows that $\{10\bar{1}2\}$ twins reorient around $\langle 1\bar{2}10 \rangle$ by 86° (Table 1). It is beneficial to the motivation of $\{10\bar{1}2\}$ twin when tensile direction is parallel to the c -axis. However, when the loading changes to the opposite direction, namely the compression direction, the $\{10\bar{1}2\}$ twin area formed before is under severe loading perpendicular to the c -axis, resulting in a 86.3° rotation of the basal plane once again and making it a recovery in crystal orientation, which keeps a delicate balance between twin and detwin. In this study, with different loading numbers, samples formed in dislocation–twinning–detwinning–dislocation and twinning–detwinning processes, but only sample 2 had more twins, leading to the discrepancy of strength and toughness in specimens. LI et al [24] found that twinning was predominated in the deformation mechanism when the plastic stress amplitude value is more than 0.5%. However, the stress amplitude value below it belongs to the range of low cycle fatigue, accounting for the low twinning portion in magnesium in high cycle fatigue, which corresponds to the experimental results.

After tension to failure, the macroscopic tensile fracture morphologies in the final fracture zone of the

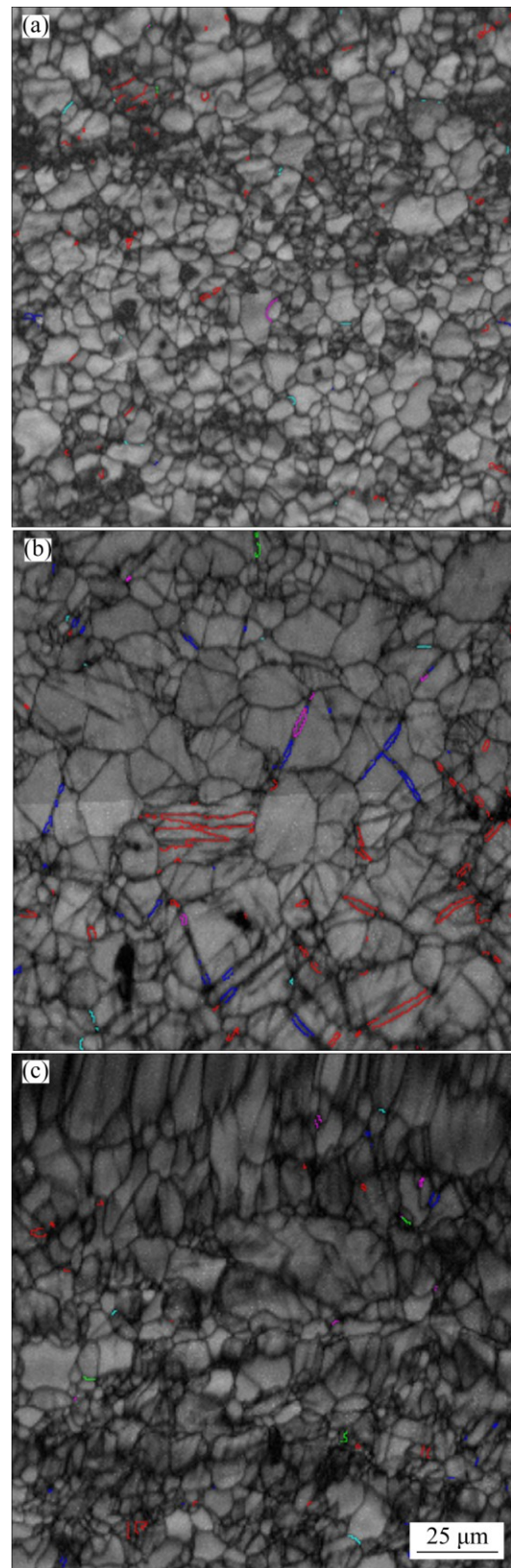


Fig. 5 EBSD micrographs of samples after fatigue tests ($\{10\bar{1}2\}$ twins and other twinning types are plotted in (a), (b) and (c) with different colors. Different types of twins are shown in Table 1 with corresponding colorful lines): (a) 10^4 ; (b) 10^6 ; (c) None

Table 1 Marks in different types of twins in EBSD images

Twinning type	Twinning plane	Misorientation/axis	Legend
Tension twin	$\{10\bar{1}2\}$	$86^\circ/\langle 1\bar{2}10\rangle$	Red
Compression twin	$\{10\bar{1}1\}$	$56^\circ/\langle 1\bar{2}10\rangle$	Magenta
	$\{10\bar{1}3\}$	$64^\circ/\langle 1\bar{2}10\rangle$	Green
Secondary twin	$\{10\bar{1}1\} - \{10\bar{1}2\}$	$38^\circ/\langle 1\bar{2}10\rangle$	Blue
	$\{10\bar{1}3\} - \{10\bar{1}2\}$	$22^\circ/\langle 1\bar{2}10\rangle$	Cyan

samples in low ($\times 400$) and high ($\times 1600$) resolutions are shown in Fig. 6. Large area of fatigue striations and cleavage fracture in samples appeared, as well as the

shallower dimples. The dimple diameters of samples 1, 2 and 3 are 14.8, 31.2 and 8.5 μm , respectively (calculated by the mean value of ten dimples selected randomly in the pictures). The fracture undergoes three conventional parts, i.e., the crack initiation area, the fatigue propagation region and the final fracture zone shown in Fig. 7(a). LV et al [25] reported that fatigue crack initiation was dominated by dislocation slips at low strain amplitudes and by twinning–detwinning process at high strain amplitudes. Surprisingly, the essence in the interrelation between loading cycle and crack initiation in this paper gradually emerges. The occurrence of the twins gives rise to crack initiation towards the end of the

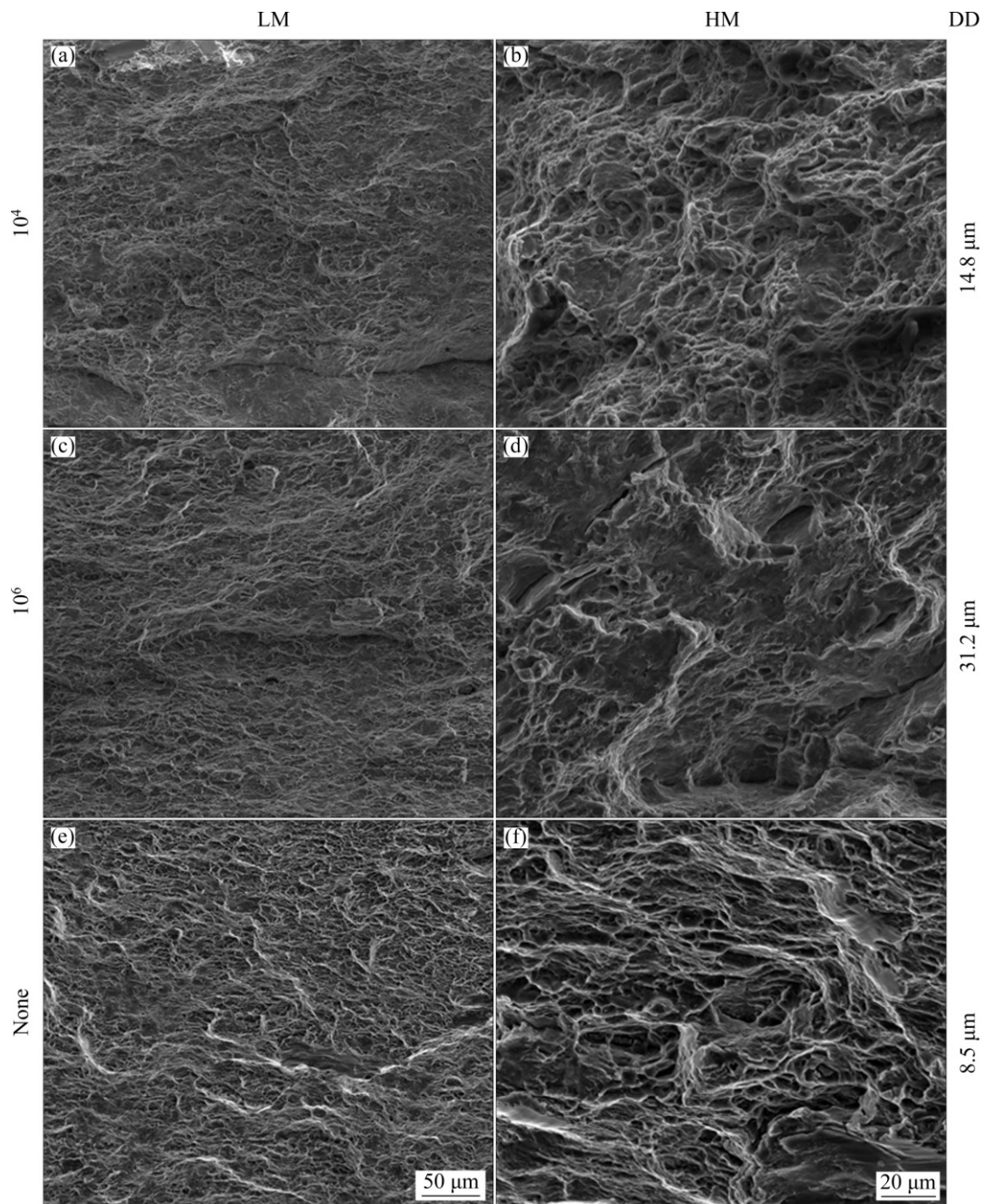


Fig. 6 Low (a, c, e) and high (b, d, f) magnification (LM and HM) macro-morphologies of tensile fracture in final fracture zone (Dimple diameter (DD) was calculated by mean value of ten dimples selected randomly in right column above)

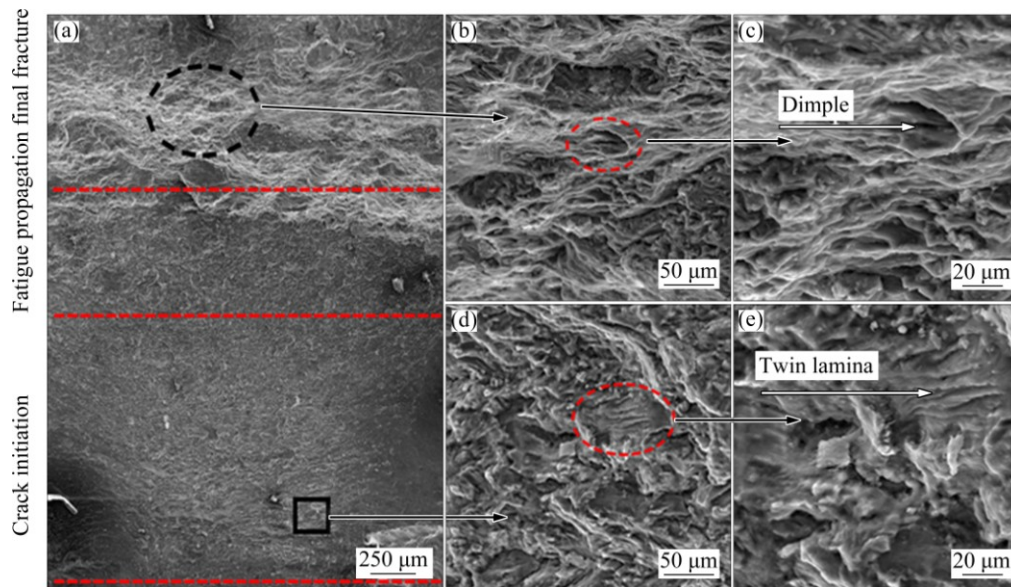


Fig. 7 SEM images of fatigue initiation, propagation and final fracture from sample 2 after fatigue test: (a) Fatigue damage occurrence labeled as crack initiation, propagation and final fracture; (b, d) Dimple-like topographies at bottom of specimen seen in high magnification SEM observations; (c, e) High magnification SEM images from crack initiation region showing existence of lamellar structure due to twinning

fatigue life. The fatigue cracks occurred nearby the specimen surface and slowly spread to central. After the loading cycled to some degree, it finally cracked.

It has gained general acceptance that fatigue crack initiation depended on the consequence of competition between twinning–detwinning process and dislocation slips in different loading cycles. In order to reveal the interactions between twin and dislocation, a close examination at a higher magnification was made by SEM (Figs. 7(b)–(e)). Fatigue crack indeed initiated from near surface defects and the fracture surfaces have a set of twin laminae near the initiation zone. In other words, the shallower dimple-like topography does not exist too much near the initiation zone. On the contrary, it comes out in the final fracture area where the cracks meet, which causes a powerful concentration of the stress, thus giving a rapid failure of the samples. Moreover, different loading cycles for magnesium alloys provide one insight into the fatigue mechanisms governing fatigue crack initiation and propagation. Crack propagation was truly related to the deformation twins at different loading cycles, which is consistent with the observation in Ref. [26].

4 Conclusions

1) Due to different loading cycles on specimens, the twinning volume fraction of the samples is different after fatigue deformation. It increases from 8% to 21% simultaneously with the cycles rising from 10^4 to 10^6 . After a tension–compression cyclic deformation, the

main $\{10\bar{1}2\}$ tension twin, a few $\{10\bar{1}1\}$ compression twinning and $\{10\bar{1}1\}$ – $\{10\bar{1}2\}$ secondary twinning generated simultaneously to a certain degree.

2) Samples formed in dislocation–twinning–detwinning–dislocation and twinning–detwinning processes. The interrelationship between twinning and detwinning makes $\{10\bar{1}2\}$ twins in fatigue samples a balance. The volume fractions of $\{10\bar{1}2\}$ twins in samples 1, 2 and 3 are 8%, 21% and 4%, respectively.

3) From the analysis of the fatigue fracture of the samples, it can be well found that there are larger areas of cleavage fracture in sample 2 than that in samples 1 and 3, and so are the shallower dimples. The crack process caused by cyclic loading undergoes three parts: crack initiation, propagation and final fracture. The twin laminae are likely to occur in the crack initiation zone while dimples are in the final fracture region. The dimple diameters of samples 1, 2 and 3 are about 14.8, 31.2 and 8.5 μm , respectively.

4) The fatigue strength and elongation of the samples tend to decrease because of the occurrence of twinning laminae induced by the cycle loadings.

References

- [1] FAN C L, CHEN D L, LUO A A. Dependence of the distribution of deformation twins on strain amplitudes in an extruded magnesium alloy after cyclic deformation [J]. *Materials Science and Engineering A*, 2009, 519(1–2): 38–45.
- [2] ZHENG X Y, LEE H, WEISGRABER T H, SHUSTEFF M, DEOTTE J, DUOSS E B, KUNTZ J D, BIENER M M, GE Q, JACKSON J A, KUCHEYEV S O, FANG N X, SPADACCINI C M.

- Ultralight, ultrastiff mechanical metamaterials [J]. *Science*, 2014, 344(6190): 1373–1377.
- [3] LUO A A. Magnesium: Current and potential automotive applications [J]. *JOM*, 2002, 54(2): 42–48.
- [4] POLLOCK T M. Weight loss with magnesium alloys [J]. *Science*, 2010, 328(5981): 986–987.
- [5] MORITA S, OHNO N, TAMAI F, KAWAKAMI Y. Fatigue properties of rolled AZ31B magnesium alloy plate [J]. *Transactions of Nonferrous Metals Society of China*, 2010, 20(2): 523–526.
- [6] CHAMOS A N, PANTELAKIS S G, HAIDEMENOPOULOS G N, KAMOUTSI E. Tensile and fatigue behaviour of wrought magnesium alloys AZ31 and AZ61 [J]. *Fatigue & Fracture of Engineering Materials and Structures*, 2008, 31(9): 812–821.
- [7] FONTE M A, FREITAS M M. Semi-elliptical fatigue crack growth under rotating or reversed bending combined with steady torsion [J]. *Fatigue and Fracture of Engineering Materials and Structures*, 2008, 20(6): 895–906.
- [8] HOSSEINI S, LIMOOEI M B. Investigation of fatigue behaviour and notch sensitivity of Ti–6Al–4V [J]. *Applied Mechanics & Materials*, 2011: 80–81(1): 7–12.
- [9] YANG F, YIN S M, LI S X, ZHANG Z F. Crack initiation mechanism of extruded AZ31 magnesium alloy in the very high cycle fatigue regime [J]. *Materials Science and Engineering A*, 2008, 491(1): 131–136.
- [10] PARK S H, HONG S G, BANG W, LEE C S. Effect of anisotropy on the low-cycle fatigue behavior of rolled AZ31 magnesium alloy [J]. *Materials Science and Engineering A*, 2010, 527(3): 417–423.
- [11] JÄGER A, LUKÁČ P, GÄRTNEROVÁ V, BOHLEN J, KAINER K U. Tensile properties of hot rolled AZ31 Mg alloy sheets at elevated temperatures [J]. *Journal of Alloys and Compounds*, 2004, 378(1–2): 184–187.
- [12] ZÚBEROVÁ Z, KUNZ L, LAMARK T T, ESTRIN Y, JANEČEK M. Fatigue and tensile behavior of cast, hot-rolled, and severely plastically deformed AZ31 magnesium alloy [J]. *Metallurgical and Materials Transactions A*, 2007, 38(9): 1934–1940.
- [13] CHINO Y, KIMURA K, HAKAMADA M, MABUCHI M. Mechanical anisotropy due to twinning in an extruded AZ31 Mg alloy [J]. *Materials Science and Engineering A*, 2008, 485(1): 311–317.
- [14] XIONG Yin, YU Qin, JIANG Yan-yao. Multiaxial fatigue of extruded AZ31B magnesium alloy [J]. *Materials Science and Engineering A*, 2012, 546(6): 119–128.
- [15] KOIKE J, OHYAMA R. Geometrical criterion for the activation of prismatic slip in AZ61 Mg alloy sheets deformed at room temperature [J]. *Acta Materialia*, 2005, 53(7): 1963–1972.
- [16] YI S, BOHLEN J, HEINEMANN F, LETZIG D. Mechanical anisotropy and deep drawing behaviour of AZ31 and ZE10 magnesium alloy sheets [J]. *Acta Materialia*, 2010, 58(2): 592–605.
- [17] YI S B, DAVIES C J, BROKMEIER H G, BOLMARO R E, KAINER K U. Deformation and texture evolution in AZ31 magnesium alloy during uniaxial loading [J]. *Acta Materialia*, 2006, 54(2): 549–562.
- [18] LOU X Y, LI M, BOGER R K, AGNEW S R, WAGONER R H. Hardening evolution of AZ31B Mg sheet [J]. *International Journal of Plasticity*, 2007, 23(1): 44–86.
- [19] DIXIT N, XIE K Y, HEMKER K J, RAMESH K T. Microstructural evolution of pure magnesium under high strain rate loading [J]. *Acta Materialia*, 2015, 87: 56–67.
- [20] WU Zhao-xuan, CURTIN W A. The origins of high hardening and low ductility in magnesium [J]. *Nature*, 2015, 526(7571): 62–67.
- [21] BETTLES C, GIBSON M. Current wrought magnesium alloys: Strengths and weaknesses [J]. *JOM*, 2005, 57(5): 46–49.
- [22] LI B, MA E, RAMESH K T. Dislocation configurations in an extruded ZK60 magnesium alloy [J]. *Metallurgical and Materials Transactions A*, 2008, 39(11): 2607–2614.
- [23] PARTRIDGE P G. Cyclic twinning in fatigued close-packed hexagonal metals [J]. *Philosophical Magazine*, 1965, 119(12): 1043–1054.
- [24] LI Qi-zhen, YU Qin, ZHANG Ji-xi, JIANG Yan-yao. Effect of strain amplitude on tension-compression fatigue behavior of extruded Mg6Al1ZnA magnesium alloy [J]. *Scripta Materialia*, 2010, 62(10): 778–781.
- [25] LV F, YANG F, DUAN Q Q, ZHANG Z F. Fatigue properties of rolled magnesium alloy (AZ31) sheet: Influence of specimen orientation [J]. *International Journal of Fatigue*, 2011, 33(5): 672–682.
- [26] MATSUZUKI M, HORIBE S. Analysis of fatigue damage process in magnesium alloy AZ31 [J]. *Materials Science and Engineering A*, 2009, 504(1): 169–174.

高周疲劳试验中 AZ31 镁合金组织和性能的演变特征

余江平, 张喜燕, 舒洋, 谭力, 尹瑞森

重庆大学 材料科学与工程学院, 重庆 400030

摘要: 利用扫描电镜和电子背散射衍射技术研究 AZ31 镁合金在高周疲劳试验中不同循环周次(包括 10^4 (样品 1)、 10^6 (样品 2)和无(样品 3 无疲劳试验))条件下的组织和性能的演变规律。结果表明, 经拉压循环变形后, 产生了大量 $\{10\bar{1}2\}$ 拉伸孪晶, 还产生了少量的 $\{10\bar{1}1\}$ 拉伸孪晶和 $\{10\bar{1}1\}-\{10\bar{1}2\}$ 二次孪晶。样品 1, 2 和 3 中 $\{10\bar{1}2\}$ 拉伸孪晶的体积分数分别为 8%、21%和 4%。疲劳断口分析发现大面积疲劳辉纹和理解断裂的区域, 韧窝直径大小随着加载次数的增加而增大。孪晶片层容易产生于裂纹萌生区, 韧窝则在终断区产生。样品 1、2 和 3 的韧窝尺寸分别为 14.8、31.2 和 8.5 μm 。样品的疲劳强度和伸长率随着加载次数增加稍有降低。

关键词: AZ31 合金; 疲劳变形; 显微组织演变; 断口形貌

(Edited by Wei-ping CHEN)